BIOCHEMISTRY
including biophysical chemistry & molecular biology

Article

pubs.acs.org/biochemistry

Molecular Differences between a Mutase and a Phosphatase: Investigations of the Activation Step in *Bacillus cereus* Phosphopentomutase

T. M. Iverson,*[,†,‡] Timothy D. Panosian,[†,∥] William R. Birmingham,[‡] David P. Nannemann,[§] and Brian O. Bachmann[‡,§]

[†]Department of Pharmacology and [‡]Department of Biochemistry, Vanderbilt University Medical Center, Nashville, Tennessee 37232, United States

[§]Department of Chemistry, Vanderbilt University, Nashville, Tennessee 37235, United States

Supporting Information

ABSTRACT: Prokaryotic phosphopentomutases (PPMs) are di-Mn^{2+} enzymes that catalyze the interconversion of α-D-ribose 5-phosphate and α-D-ribose 1-phosphate at an active site located between two independently folded domains. These prokaryotic PPMs belong to the alkaline phosphatase superfamily, but previous studies of *Bacillus cereus* PPM suggested adaptations of the conserved alkaline phosphatase catalytic cycle. Notably, *B. cereus* PPM engages substrates when the active site nucleophile, Thr-85, is phosphorylated. Further, the phosphoenzyme is stable throughout purification and crystallization. In contrast, alkaline phosphatase engages substrates when the active site nucleophile is dephosphorylated, and the phosphoenzyme reaction intermediate is only stably trapped in a catalytically compromised enzyme. Studies were undertaken to understand the divergence of these mechanisms. Crystallographic and biochemical investigations of the PPM^{T85E} phosphomimetic variant and the neutral corollary PPM^{T85Q} determined that the side chain of Lys-240 underwent a change in conformation in response to active site charge, which modestly influenced the affinity for the small molecule activator α-D-glucose 1,6-bisphosphate. More strikingly, the structure of unphosphorylated *B. cereus* PPM revealed a dramatic change in the interdomain angle and a new hydrogen bonding interaction between the side chain of Asp-156 and the active site nucleophile, Thr-85. This hydrogen bonding interaction is predicted to align and activate Thr-85 for nucleophilic addition to α-D-glucose 1,6-bisphosphate, favoring the observed equilibrium phosphorylated state. Indeed, phosphorylation of Thr-85 is severely impaired in the PPM^{D156A} variant even under stringent activation conditions. These results permit a proposal for activation of PPM and explain some of the essential features that distinguish between the catalytic cycles of PPM and alkaline phosphatase.

Phosphopentomutases (PPMs) interconvert α-D-ribose 5-phosphate (ribose 5-phosphate) and α-D-ribose 1-phosphate (ribose 1-phosphate). Physiologically, this allows products of RNA breakdown to be used in glycolysis or purine and pyrimidine synthesis.[1] PPM activity has been observed in both prokaryotes and eukaryotes;[2,3] however, sequence and structural comparisons indicate that prokaryotic and eukaryotic PPMs are unrelated.[4,5]

Bacterial PPMs belong to the alkaline phosphatase superfamily, a large and diverse family of dimetalloenzymes that catalyze phosphoryl or sulfonyl transfer via a conserved reaction cycle.[4] Indeed, the structure of *Bacillus cereus* PPM is dominated by a core domain with a fold related to alkaline phosphatase; however, it also contains a cap domain that is unique to phosphopentomutases (Figure 1).[6] The active site is located at the interface between these two domains. Previous structure-based enzymology of *B. cereus* PPM[6] revealed numerous architectural and mechanistic parallels between PPM and alkaline phosphatase. The active sites of PPM and alkaline phosphatase exhibit virtually identical geometries, with both containing a catalytic nucleophile (Thr-85 in *B. cereus* PPM and Ser-102 in *Escherichia coli* alkaline phosphatase[7]) and a dimetallo center (di-Mn^{2+} in *B. cereus* PPM and di-Zn^{2+} in *E. coli* alkaline phosphatase[8]). The coordinating residues to the dimetallo center are absolutely conserved in both sequence and structure with the exception of an additional ligand within the *B. cereus* active site, Asp-156, that is located on the unique cap domain.[6,9] Accordingly, the alkaline phosphatase reaction cycle was used as a starting point for developing a reaction mechanism specific for PPM.[6]

Interestingly, *B. cereus* PPM appears to have several mechanistic adaptations as compared to the remainder of the alkaline phosphatase superfamily (Figure 2A,B). The most surprising difference between PPM and alkaline phosphatase is that the active site phosphorylation status of the catalytic form of the enzymes differs. In PPM, the substrate is acted upon by the enzyme in which the catalytic nucleophile, Thr-85 in *B. cereus* PPM, is phosphorylated (p-Thr-85). The catalytic cycle proceeds through an intermediate with an unphosphorylated enzyme and a doubly phosphorylated substrate.[6] Conversely, in

Received: November 29, 2011
Revised: January 25, 2012
Published: February 13, 2012

dx.doi.org/10.1021/bi201761h | *Biochemistry* 2012, 51, 1964−1975

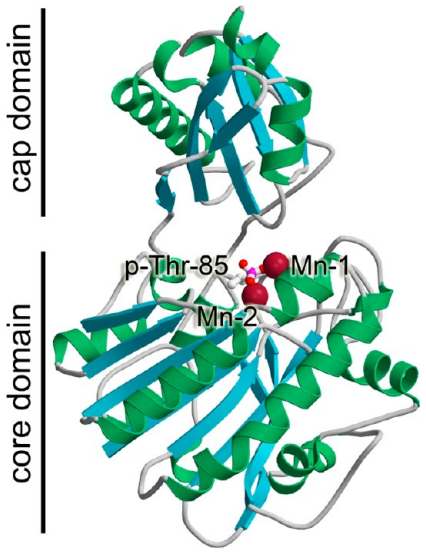

Figure 1. Structure of phosphorylated *B. cereus* PPM. The structure of *B. cereus* PPM is colored by secondary structural elements, with α-helices in green and β-strands in cyan. The active site contains two Mn^{2+} ions, colored burgundy. The phosphorylated catalytic nucleophile, p-Thr-85, is shown as a stick model with carbon colored gray, oxygen red, and phosphorus magenta.

alkaline phosphatases, the substrates encounter an enzyme in which the catalytic nucleophile, Ser-102 in the *E. coli* alkaline phosphatase, is dephosphorylated. The catalytic cycle proceeds through a transient intermediate in which the enzyme is phosphorylated and the substrate is dephosphorylated.[9,10] This key difference requires that PPM use an altered entry point to the catalytic cycle in comparison to other characterized members of the alkaline phosphatase superfamily, but overall, the catalytic cycle itself is conserved (Figure 2A,B).

Phosphorylation of PPM requires a dedicated chemical activation step, which is achieved in vitro using the small molecule activator α-D-glucose 1,6-bisphosphate (glucose 1,6-bisphosphate). Because this activation is one requirement for the mechanistic divergence between PPM and alkaline phosphatase, studies were undertaken to identify the mechanisms of the activation process. Structures of a phosphomimetic variant of PPM (PPM^{T85E}), the neutral corollary (PPM^{T85Q}), and a fully unphosphorylated form of PPM suggest a mechanism favoring activation that is unique to phosphopentomutases within the alkaline phosphatase superfamily.

EXPERIMENTAL PROCEDURES

Materials. Unless otherwise stated, all materials were of the highest grade commercially available and were used without further purification.

Cloning, Expression, and Purification. N-Terminally hexahistidine-tagged *B. cereus* PPM was cloned, expressed, and purified as described previously.[11] Site-directed substitutions were prepared from the gene contained in plasmid pET28+[11] using the QuikChange mutagenesis kit (Stratagene). Primers for the PPM^{T85E} variant were GCAAGAGAAATCTACTGGTAAAGATGAAATGACAGGTCACTGGGAAATCATGGGCC and GGCCCATGATTTCCCAGTGACCTGTCATTTCATCTTTACCAGTAGATTTCTCTTGC, for the PPM^{T85Q} variant GCAAGAGAAATCTACTGGTAAAGATCAAATGACAGGTCACTGGGAAATCATGGGCC and

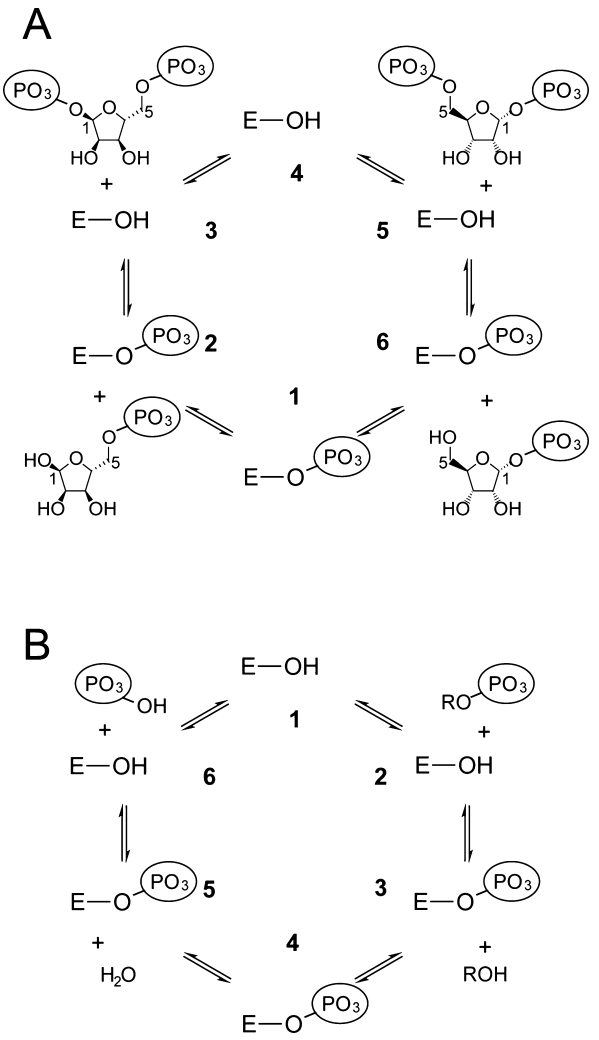

Figure 2. Proposed catalytic cycles of PPM and alkaline phosphatase. (A) Proposed catalytic cycle for the interconversion of ribose 5-phosphate and ribose 1-phosphate by *B. cereus* PPM . This six-step mechanism is extrapolated from the alkaline phosphatase mechanism (see panel B[6]) and is discussed from step 1 to 6, although all steps are reversible. In step 1, the enzyme is phosphorylated and active. In step 2, the substrate, ribose 5-phosphate encounters the active enzyme. In step 3, a phosphoryl group is transferred from the enzyme to the 1-OH of ribose 5-phosphate, resulting in a ribose 1,5-bisphosphate chemical intermediate and an unphosphorylated enzyme intermediate. In step 4, the ribose 1,5-bisphosphate is reoriented in the enzyme active site. In step 5, the reoriented ribose 1,5-bisphosphate encounters the unphosphorylated enzyme. In step 6, a phosphoryl group is transferred from ribose 1,5-bisphosphate back to the enzyme. The end result is a ribose 1-phosphate chemical product and a phosphorylated, active enzyme. (B) Proposed mechanism for alkaline phosphatase. Alkaline phosphatase is a promiscuous enzyme that acts upon a variety of phosphorylated substrates and can use either water or a second organic molecule as a phosphate acceptor; a representative phosphatase reaction, in which water is the phosphate acceptor, is shown. Step 1 of this six-step mechanism starts with active, dephosphorylated enzyme (compare to step 4 of the PPM mechanism). In step 2, the phosphorylated substrate enters the active site (compare to step 5 of the PPM mechanism). In step 3, a phosphoryl group is transferred from the substrate to the enzyme, resulting in a dephosphorylated substrate and a phosphorylated enzyme intermediate (compare to step 6 of the PPM mechanism). In step 4, the dephosphorylated chemical substrate dissociates from the enzyme (compare to step 1 of the PPM mechanism). In step 5, a water molecule enters the active site and encounters the phosphorylated enzyme (compare to step 2 of the

dx.doi.org/10.1021/bi201761h | *Biochemistry* 2012, 51, 1964−1975

Figure 2. continued

PPM mechanism). In step 6, the phosphoryl group is transferred from the enzyme to the water molecule to release phosphate (compare to step 3 of the PPM mechanism). The end result is a dephosphorylated substrate, a free phosphate, and a dephosphorylated, active enzyme.

GGCCCATGATTTCCCAGTGACCTGTCATTTGATCTTTACCAGTAGATTTCTCTTGC, for the PPM^{K240A} variant CGATGTAATTGCTATTGGTGCAATCTCTGATATTTATGATGG and CCATCATAAATATCAGAGATTGCACCAATAGCAATTACATCG, and for the PPM^{D156A} variant CAGGCTCTTTAATCGTTTATACTTCTGCTGCCAGCGTATTGCAAATTGCAGCACACGAAG and CTTCGTGTGCTGCAATTTGCAATACGCTGGCAGCAGAAGTATAAACGATTAAAGAGCCTG.

Wild-type and variant PPMs were expressed and purified using a previously reported protocol.[11] Briefly, plasmids were transformed into *E. coli* BL21(DE3). The cells were grown in LB medium at 37 °C and induced with 0.3 mM IPTG after the OD_{600} had reached 0.4−0.6. Cells were disrupted by sonication, and the protein was purified from the clarified lysate using two chromatographic steps. The first step used a HisTrap (GE Healthcare) Ni affinity column, in which the protein was bound to the column in 50 mM Tris-HCl, 200 mM NaCl, 1 mM $MnCl_2$, and 10 mM imidazole (pH 7.5) and eluted from the column in 50 mM Tris-HCl, 200 mM NaCl, 1 mM $MnCl_2$, and 300 mM imidazole (pH 7.5). The hexahistidine affinity tag was then removed by overnight thrombin cleavage at 22 °C in buffer containing 50 mM Tris-HCl, 200 mM NaCl, and 1 mM $MnCl_2$ (pH 7.5). The protein was further purified using size exclusion chromatography on a Superdex 200 10/300 GL column (GE Healthcare) equilibrated with 25 mM Tris-HCl and 1 mM $MnCl_2$ (pH 7.5).

Crystallization, Data Collection, and Structure Determination of Wild-Type and Variant PPM in the $P2_1$ Crystal Form. Crystals of PPM variants were grown using the hanging drop vapor diffusion method using a modification of the crystallization conditions described previously.[11] All proteins were at a concentration of 10 mg/mL buffered in 25 mM Tris-HCl and 1 mM $MnCl_2$ (pH 7.5). Crystals of the PPM^{T85E} variant grew over a reservoir solution containing 100 mM Bis-Tris (pH 5.5), 50 mM $MnCl_2$, 17% polyethylene glycol 3350, and 75 mM NH_4CH_3COO. Crystals of the PPM^{T85Q} variant crystallized over a reservoir solution containing 100 mM Bis-Tris (pH 5.5), 50 mM $MnCl_2$, 13% polyethylene glycol 3350, and 75 mM NH_4CH_3COO. Cocrystals of each variant with glucose 1,6-bisphosphate were prepared by soaking fully formed crystals in 5 mM glucose 1,6-bisphosphate. For the costructure of activated wild-type PPM bound to glucose 1,6-bisphosphate, PPM was incubated with 5 mM glucose 1,6-bisphosphate in 25 mM Tris-HCl (pH 7.4) and 1 mM $MnCl_2$ at room temperature for 30 min prior to setting drops. Crystals grew over a reservoir solution containing 100 mM Bis-Tris (pH 5.5), 50 mM $MnCl_2$, 14% polyethylene glycol 3350, and 50 mM NH_4CH_3COO. Fully formed crystals of the activated enzyme were then soaked in a solution containing all of the crystallization components and 5 mM glucose 1,6-bisphosphate for 1 h at 18 °C. All crystals were cryoprotected in a solution that was 70% (v/v) reservoir solution and 30% (v/v) glycerol prior to being cryocooled in liquid nitrogen.

Crystal quality was assessed at Stanford Synchrotron Radiation Lightsource beamline 9-2 and Advanced Photon Source (APS) beamline 21-ID-G; all data sets were collected on APS beamline 21-ID-G. Data were processed using the HKL2000[12] and CCP4[13] suites of programs (Table 1). Crystals grown from these conditions formed in primitive monoclinic space group $P2_1$. The unit cell dimensions of the wild type and

Table 1. Data Collection and Refinement Statistics for Wild-Type PPM and Its Variants Crystallized in Space Group $P2_1$

	PPM^{T85E} variant	PPM^{T85E} variant soaked with glucose 1,6-bisphosphate	PPM^{T85Q} variant	PPM^{T85Q} variant soaked with glucose 1,6-bisphosphate	wild-type, activated PPM soaked with glucose 1,6-bisphosphate
PDB entry	3UN5	3UNY	3UN2	3UN3	3UO0
			Data Collection		
resolution (Å)[a]	20−1.8 (1.86−1.8)	20−1.95 (2.01−1.95)	20−1.8 (1.86−1.8)	20−1.8 (1.86−1.8)	20−2.3 (2.38−2.3)
unit cell parameters	a = 106.4 Å	a = 106.6 Å	a = 91.9 Å	a = 91.6 Å	a = 91.8 Å
	b = 76.8 Å	b = 76.8 Å	b = 76.7 Å	b = 76.8 Å	b = 77.1 Å
	c = 182.8 Å	c = 182.3 Å	c = 107.2 Å	c = 106.8 Å	c = 108.3 Å
	β = 106.0°	β = 106.1°	β = 108.7°	β = 108.6°	β = 108.9°
total no. of reflections	896177	686614	461139	424067	231036
no. of unique reflections	254487	206406	130700	125668	63622
I/σ^a	22.3 (2.5)	13.9 (2.6)	22.5 (2.6)	19.6 (2.2)	15.8 (3.2)
completeness (%)[a]	97.4 (84.8)	99.2 (95.9)	97.5 (81.4)	96.3 (77.4)	99.7 (97.8)
R_{sym}[a,b]	0.06 (0.34)	0.08 (0.34)	0.06 (0.36)	0.07 (0.39)	0.08 (0.36)
			Model Refinement		
no. of reflections in test set	12792	10161	6535	5997	4517
R_{cryst}[c]	0.179	0.167	0.180	0.165	0.173
R_{free}[d]	0.207	0.199	0.208	0.191	0.225

[a]Values in parentheses are for the highest-resolution shell. [b]$R_{sym} = \sum|I_{obs} - I_{avg}|/I_{avg}$. [c]$R_{cryst} = (\sum||F_{obs}| - |F_{calc}||)/\sum|F_{obs}|$. [d]$R_{free}$ is calculated using the same equation as R_{cryst} using a subset of reflections omitted from refinement and reserved in the test set of data.

the PPM^{T85Q} variant were similar to those previously reported.[6] Accordingly, initial phases were determined by rigid body refinement of the structure of *B. cereus* PPM [Protein Data Bank (PDB) entry 3M8W[6]] using CNS.[14] Crystals of the PPM^{T85E} variant had unit cell dimensions significantly different from those previously reported.[6] The structure of the PPM^{T85E} variant was determined with PHASER,[15] using the structure of wild-type *B. cereus* PPM (PDB entry 3M8W[6]) as the search model. Models were improved with iterative rounds of model building in COOT[16] and refinement in CNS[14] and REFMAC.[17,18] For the latter, Translation/Libration/Screw (TLS)[19] groups were assigned using the TLS Motion Determination server.[20]

Crystallization, Data Collection, and Structure Determination of Unphosphorylated PPM in the $P2_12_12_1$ Crystal Form. Crystal packing interactions in the $P2_1$ crystal form restrict the interdomain orientation (see Figure S1 of the Supporting Information). Given the possibility of interdomain rotation during catalysis, we sought to identify a new crystal form for the unphosphorylated enzyme. Accordingly, we identified a protein with a low phosphorylation level and performed sparse matrix screening. Both previous enzyme activity assays and Western analyses suggested that different protein preparations of PPM varied in the level of phosphorylation of Thr-85 (unpublished observations). Some of the variables influencing the degree of phosphorylation may include the length of time taken during the overall purification process, the age of the protein preparation, and the storage temperature. Sparse matrix screening was performed with enzyme preparations comparable to those for which Western analyses did not detect measurable p-Thr, and the preparations are thus expected to have low levels of phosphorylation (<5%) in sitting drops with a Mosquito drop setter (TTP LabTech) by mixing 200 nL of protein and 200 nL of reservoir solution and equilibrating over 100 μL of reservoir solution. The crystals used for data collection were grown using the hanging drop vapor diffusion method by equilibrating either 1 μL of 10 mg/mL unphosphorylated *B. cereus* PPM [buffered in 25 mM Tris-HCl, 1 mM $MnCl_2$ (pH 7.5), 5 mM sodium orthovanadate, and 5 mM ribose 5-phosphate] and 1 μL of reservoir solution [125 mM $MnCl_2$ and 1.8 M ammonium citrate (pH 7.2)] over 1 mL of reservoir solution or 1 μL of 10 mg/mL phosphorylated *B. cereus* PPM (buffered in 25 mM Tris-HCl and 1 mM $MnCl_2$) over the same reservoir solution. Crystals were cryoprotected using a 1:1 mixture of paratone-N and mineral oil prior to being flash-cooled in liquid nitrogen.

Diffraction data were collected at 100 K on LS-CAT beamline 21-ID-G using a wavelength of 0.979 Å and a MAR 225 CCD detector. Data were processed and scaled using the HKL2000 suite of programs,[12] which demonstrated that these crystals formed in primitive orthorhombic space group $P2_12_12_1$ (Table 2). The unit cell dimensions were distinct from those observed in the previously reported $P2_1$ space group.

Structure Determination and Refinement of Phosphorylated and Unphosphorylated PPM in Space Group $P2_12_12_1$. Structures of both phosphorylated and unphosphorylated *B. cereus* PPM in space group $P2_12_12_1$ were determined by molecular replacement with PHASER[15] using the structure of *B. cereus* PPM in space group $P2_1$ (PDB entry 3M8W[11]) as the search model. The structure of the phosphorylated protein used the entire protein as the search model, while the structure of the unphosphorylated protein could be determined only when the isolated alkaline phosphatase-like core domain (residues 2–99 and 216–393) was used as the search model. The models were improved using iterative rounds of model building in COOT[16] and refinement in CNS[14] and REFMAC.[18] TLS groups for REFMAC were determined using the TLS Motion Determination server.[20] Refinement statistics for the final models are listed in Table 2. Subsequent analysis of the crystal packing interactions in the $P2_12_12_1$ crystal form confirmed that this crystal form did not restrict the orientation between domains in PPM (see Figure S1 of the Supporting Information).

Table 2. Data Collection and Refinement Statistics for Phosphorylated and Unphosphorylated PPM in Space Group $P2_12_12_1$

	phosphorylated PPM	unphosphorylated PPM
PDB entry	3TX0	3TWZ
	Data Collection	
resolution (Å)	50–1.75 (1.80–1.75)[a]	50–2.26 (2.32–2.26)[a]
unit cell parameters (Å)	a = 68.7	a = 61.0
	b = 76.6	b = 75.7
	c = 107.2	c = 95.6
resolution (Å)	50–1.75 (1.81–1.75)[a]	50–2.25 (2.33–2.25)[a]
total no. of reflections	265458	73732
no. of unique reflections	47942	19421
I/σ	17.5 (3.3)[a]	24.3 (3.5)[a]
completeness (%)	91.6 (63.4)[a]	92.1 (64.3)[a]
R_{sym}[b]	0.08 (0.33)[a]	0.07 (0.26)[a]
	Model Refinement	
no. of R_{free} reflections	2428	989
R_{cryst}[c]	0.177	0.189
R_{free}[d]	0.196	0.246

[a]Values in parentheses are for the highest-resolution shell. [b]$R_{sym} = \sum(I_i - \langle I\rangle)/\sum\langle I\rangle$, where I is ith measurement and $\langle I\rangle$ is the weighted mean of I. [c]$R_{cryst} = \sum||F_{obs}| - |F_{calc}||/\sum|F_{obs}|$. [d]$R_{free}$ is calculated using the same equation as R_{cryst} using a subset of reflections omitted from refinement and reserved in the test set of the data.

Structural Analysis and Molecular Visualization. Changes in the interdomain angle were calculated using DynDom.[21] Structural comparisons were performed in O.[22] Figures 1, 3, and 5–7 were prepared using Molscript,[23] Bobscript,[24] and Raster3D.[25] Video 1 of the Supporting Information was made using PyMol.[26]

Hypoxanthine Consumption Assay for PPM Activity. The activity of wild-type PPM and the PPM^{T85Q}, PPM^{T85E}, PPM^{K240A}, and PPM^{D156A} variants was measured in a tandem assay with human purine nucleoside phosphorylase and measured by hypoxanthine consumption by xanthine oxidase; both of these enzymes were expressed and purified using previously reported protocols.[27,28] In this assay, ribose 1-phosphate formed by PPM was consumed by a catalytic excess of purine nucleoside phosphorylase in the presence of hypoxanthine to form inosine. Inosine formation was assessed at end points by measuring hypoxanthine consumption using a typical hypoxanthine detection assay[29] containing xanthine oxidase and iodonitrotetrazolium chloride, which produces a colored formazan, quantified at 546 nm.

All reactions were performed in 100 μL volumes in 96 well plates. Wild-type or variant PPM buffered in 25 mM Tris-HCl (pH 8) and 0.1 mM $MnCl_2$ at a concentration 10-fold higher

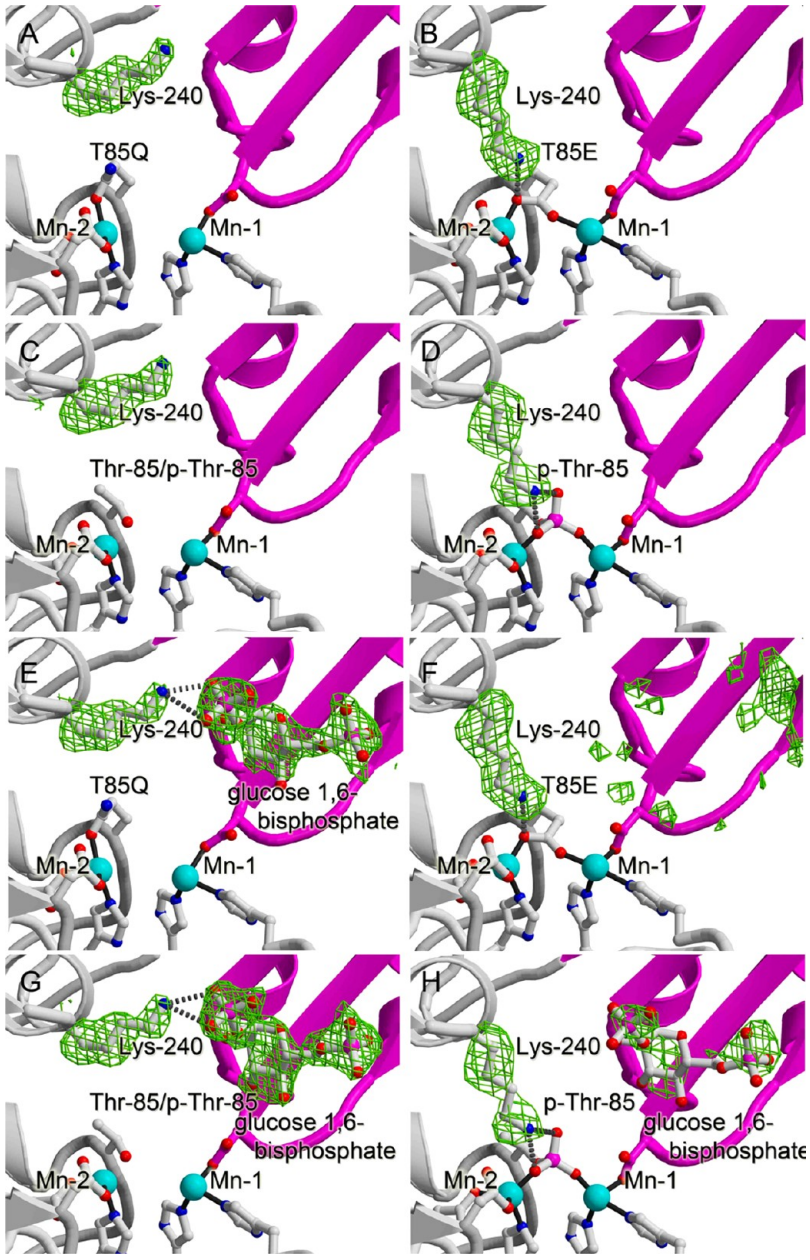

Figure 3. Comparison of the position of the Lys-240 side chain and the binding of glucose 1,6-bisphosphate in the PPM^{T85E} and PPM^{T85Q} variant enzymes and in the unactivated and activated wild-type enzymes. Carbons are colored gray, nitrogens blue, and oxygens red, and the Mn^{2+} ions are shown as cyan spheres. Metal ligations (distances of <2.2 Å) are shown as solid black lines, and hydrogen bonding interactions are shown as dashed gray lines. All figure panels show the final model superimposed with $|F_o| - |F_c|$ simulated annealing electron density (green mesh) calculated after the omission of both the Lys-240 side chain (A–H) and glucose 1,6-bisphosphate (E–H) and displayed at 3σ. The side chain of Asp-286, a metal ligand to Mn-2, has been omitted from all figure panels for the sake of clarity. (A) Structure of PPM^{T85Q} crystallized without glucose 1,6-bisphosphate. (B) Structure of PPM^{T85E} crystallized without glucose 1,6-bisphosphate. (C) Structure of unactivated PPM (low phosphorylation level, PDB entry 3M8W[6]) crystallized without glucose 1,6-bisphosphate. Thr-85 is in a mixed state in this structure with an estimated occupancy of the phosphate of 30%. The position of the phosphate has been omitted for the sake of clarity. (D) Structure of activated PPM (high phosphorylation level, PDB entry 3M8Y[6]) crystallized without glucose 1,6-bisphosphate. (E) Structure of PPM^{T85Q} crystallized with glucose 1,6-bisphosphate. The estimated occupancy of the glucose 1,6-bisphosphate is 75%. (F) Structure of PPM^{T85E} crystallized with glucose 1,6-bisphosphate. The electron density was not sufficient to include glucose 1,6-bisphosphate in the model, even at low occupancy. (G) Structure of unactivated PPM (low phosphorylation level, PDB entry 3OTY[6]) crystallized with glucose 1,6-bisphosphate. The estimated occupancy of the phosphate is 30%, and the estimated occupancy of glucose 1,6-bisphosphate is 75%. The position of the phosphate has been omitted for the sake of clarity. (H) Structure of activated PPM crystallized with glucose 1,6-bisphosphate. The estimated occupancy of the phosphate is 100%, and the estimated occupancy of the glucose 1,6-bisphosphate is 50%.

than that used in the assay was preactivated for 10 min at room temperature with 5 μM glucose 1,6-bisphosphate and then held at 4 °C until it was assayed. Final assay conditions were 20 nM wild-type PPM and each of the PPM variants at 50, 100, 250, or 500 nM buffered in 0.1 mM $MnCl_2$, 25 mM Tris-HCl (pH 8), 5 μM human purine nucleoside phosphorylase, 600 μM hypoxanthine, and 1 mM ribose 5-phosphate. Reactions were initiated by the addition of the substrate, ribose 5-phosphate,

dx.doi.org/10.1021/bi201761h | *Biochemistry* 2012, 51, 1964–1975

mixtures incubated for 10 min at room temperature, and then reactions quenched by addition of 5 μL of 2 M NaOH. After 20 min at room temperature, the reaction mixtures were neutralized by the addition of 5 μL of 2 M HCl; 75 μL of the quenched assay was combined with 20 μL of 0.2% Triton X-100, 7.5 mM iodonitrotetrazolium chloride, and xanthine oxidase in 25 mM Tris-HCl (pH 8). Hypoxanthine consumption was assessed on the basis of the absorbance at 546 nm in comparison to a standard curve run in parallel.

Measurement of Binding Affinity for Glucose 1,6-Bisphosphate by Intrinsic Fluorescence. The intrinsic fluorescence of protein samples was measured at 20 °C in a Cary Eclipse spectrophotometer with excitation and emission slits set to 20 nm and the detector voltage set to 675 mV. For each measurement, 114 μL of 0.5 μM wild-type or variant PPM [in buffer containing 50 mM Tris-HCl (pH 8.0) and 0.1 mM $MnCl_2$] was mixed with 6 μL of the appropriate concentration of glucose 1,6-bisphosphate immediately prior to the sample being placed into the instrument. After 1 min, the sample was excited at 280 nm and the emission spectrum read from 300 to 400 nm. Each individual sample was measured three times in immediate succession, and each data point is the average of three samples for a total of nine measurements. The concentration-dependent change in fluorescence following the addition of glucose 1,6-bisphosphate was significant for all samples tested. The K_d was calculated by plotting the change in fluorescence intensity at 350 nm against the concentration of glucose 1,6-bisphosphate and fitting to a single-binding site model with GraphPad Prism version 5.01.

Phosphothreonine Western Analysis. Either wild-type or variant PPM (2 μM) was incubated in 25 mM Tris-HCl (pH 8.0), 0.1 mM $MnCl_2$, and a varied concentration of glucose 1,6-bisphosphate at room temperature for 30 min. Samples were quenched by addition of SDS sample buffer and heating at 95 °C for 5 min before separation by sodium dodecyl sulfate–polyacrylamide gel electrophoresis and subsequent transfer to a 0.45 μm nitrocellulose membrane. Total protein was observed by Ponceau S staining, which was removed by washing with water after imaging. The membrane was blocked using Odyssey blocking buffer (LI-CORP Biosciences) overnight and incubated with an anti-phosphothreonine antibody (Cell Signaling) diluted 1:1000 in BSA-TTBS (TBS containing 0.5% BSA and 0.1% Tween 20) for 2 h at 22 °C. The membrane was then incubated for 1 h at 22 °C with an AlexaFluor680-conjugated goat anti-rabbit antibody (Invitrogen) diluted 1:20000 in BSA-TTBS and was visualized using an Odyssey Infrared Imaging System.

Phosphate Release Assay. The phosphatase activity of wild-type and variant PPM was measured using molybdate-based methods as previously described[30] with 20 nM wild-type PPM, either 1 or 5 μM PPM^{D156A}, 1 mM ribose 5-phosphate or 1 mM glucose 1,6-bisphosphate, 0.1 mM $MnCl_2$, and 25 mM Tris-HCl (pH 8). Background absorbance values from the substrate and enzyme reaction mix were subtracted from the reaction measurements, and phosphate turnover was assessed by comparison to a standard curve.

RESULTS

Structures of p-Thr-85 Phosphomimetic Mutants and the Conformation of the Lys-240 Side Chain. Previous studies of *B. cereus* PPM demonstrated that activity required phosphorylation of the catalytic nucleophile, Thr-85.[6] As a starting point to understanding how the phosphothreonine was stabilized, we sought to identify if there were structural consequences of phosphorylation. Accordingly, we engineered site-directed substitutions of the catalytic nucleophile, Thr-85, changing this residue to the phosphomimetic glutamate (PPM^{T85E}, activated mimetic) or the neutral corollary glutamine (PPM^{T85Q}, unactivated mimetic). As anticipated, neither of these variants displayed detectable phosphomutase activity (data not shown) and both displayed a monodisperse elution profile in size exclusion chromatography with an elution volume similar to that of the wild-type enzyme.

The structures of the PPM^{T85Q} and PPM^{T85E} variants (Figure 3A,B) showed that these proteins were properly folded and that neither exhibited significant backbone conformational changes when compared to the wild-type enzyme. Interestingly, the side chain of Lys-240 in the PPM^{T85Q} variant was oriented such that it contributed to the formation of a glucose 1,6-bisphosphate binding pocket (Figure 3A), a conformation that resembled that observed in the structure of unactivated PPM (Figure 3C, PDB entry 3M8W[6]). Conversely, the orientation of the side chain of Lys-240 in the PPM^{T85E} variant formed an interaction with the side chain of Glu-85 (Figure 3B), which resembles that observed in the structure of activated PPM (Figure 3D, PDB entry 3M8Y[6]). Taken together, these structures suggest that the net charge at the active site could influence the conformation of the Lys-240 side chain.

Influence of the Conformation of Lys-240 on the Affinity for the Activator Glucose 1,6-Bisphosphate. To verify that the location of the glucose 1,6-bisphosphate binding site is not altered upon mutation of the enzyme, we next determined the crystal structures of the complexes of activated wild-type PPM, the PPM^{T85Q} variant, and the PPM^{T85E} variant after they had been soaked with 5 mM glucose 1,6-bisphosphate (Figure 3E–H). In all cases, electron density for the activator (if apparent) was observed in the same location that was previously identified;[6] however, the quality of the electron density suggested different binding occupancy in each case. Clear electron density for glucose 1,6-bisphosphate was observed in the costructure of the activator with the unactivated mimetic PPM^{T85Q} (Figure 3E), and the intensity of this electron density was similar to that observed in the structure determined from crystals of unactivated PPM soaked with glucose 1,6-bisphosphate (Figure 3G, PDB entry 3OT9[6]). Conversely, virtually no electron density corresponding to the activator was observed in the costructure of glucose 1,6-bisphosphate with the PPM^{T85E} activated mimetic (Figure 3F), while only poor electron density was observed in the costructure of activated PPM soaked with glucose 1,6-bisphosphate (Figure 3H). In the former structure, coordinates for glucose 1,6-bisphosphate were not included in the final model.

Because the PPM^{T85Q} variant mimics the active site charge of the unactivated state of the enzyme, and the position of the side chain of Lys-240 may be predicted to contribute to the formation of a binding site for the activator in the absence of phosphorylation, we quantified whether this conformational change altered the binding affinity of the enzyme for the activator, glucose 1,6-bisphosphate. To assess the affinity, we took advantage of the proximity of Trp-90 to the active site and developed a fluorescence assay for monitoring ligand binding. With this assay, we measured the affinity of glucose 1,6-bisphosphate in the unactivated wild-type enzyme, the PPM^{T85Q} variant (unactivated mimetic), and the PPM^{T85E} variant (activated mimetic) (Figure 4). Measurements of the

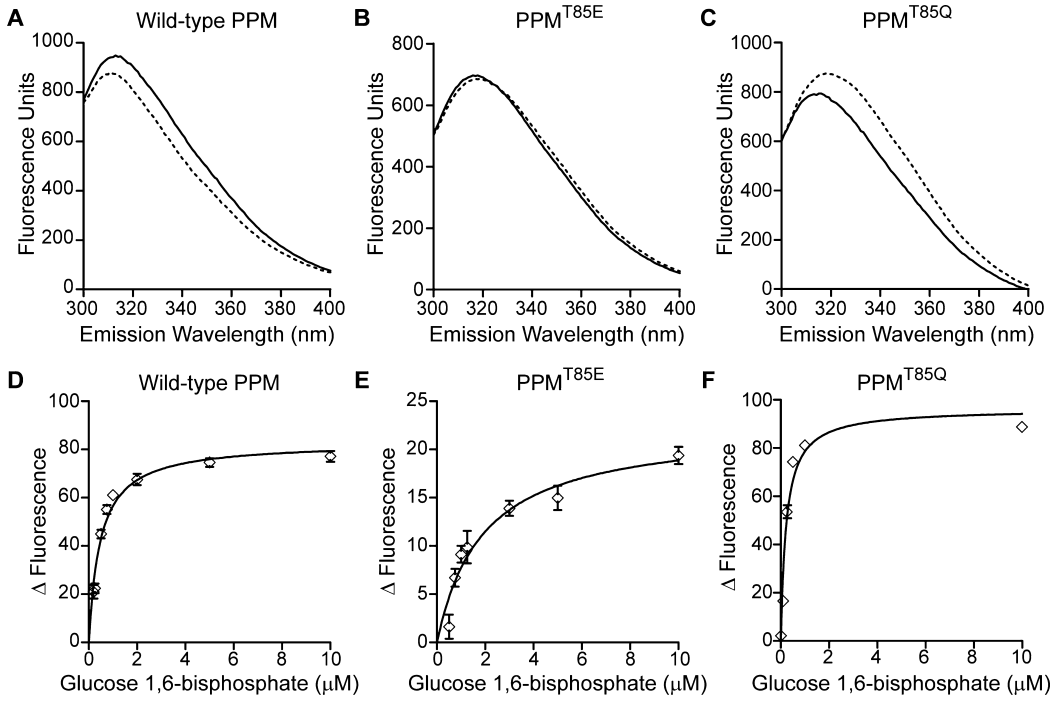

Figure 4. Changes in the intrinsic fluorescence spectra of wild-type and variant PPM following the addition of glucose 1,6-bisphosphate. (A–C) Representative spectra of (A) wild-type, unphosphorylated PPM, (B) the PPM^{T85E} variant, and (C) the PPM^{T85Q} variant recorded in the absence (—) and presence (---) of 10 μM glucose 1,6-bisphosphate. (D–F) Plots of the change in fluorescence intensity at 350 nm following the addition of glucose 1,6-bisphosphate for (D) wild-type, unphosphorylated PPM, (E) the PPM^{T85E} variant, and (F) the PPM^{T85Q} variant. Points are the average of three separately prepared samples each measured three times, and error bars are the standard deviation of the mean.

affinity on the activated wild-type enzyme were precluded because activation requires the continued presence of glucose 1,6-bisphosphate, and therefore, fully activated PPM could not be isolated from glucose 1,6-bisphosphate. Consistent with the hypothesis that the conformational change in Lys-240 alters the affinity of the enzyme for the activator, both the unactivated wild-type enzyme and the PPM^{T85Q} variant exhibited similar affinities for glucose 1,6-bisphosphate of 0.47 ± 0.04 and 0.23 ± 0.02 μM, respectively, while the PPM^{T85E} variant had a 4.5-fold lower affinity of 2.05 ± 0.39 μM.

Structural Changes in Unphosphorylated *B. cereus* PPM. Previous structures of unactivated PPM were likely determined from a mixed population of enzyme, with some of the protein phosphorylated and some unphosphorylated. In these structures, the occupancy of the Thr-85 phosphate was estimated to be 30%.[6] Determination of the structure of fully unphosphorylated *B. cereus* PPM required the identification of a new crystal form. Both phosphorylated and unphosphorylated *B. cereus* PPM could be crystallized in this new crystal form, and comparison of the two structures allowed conformational changes associated with crystal packing to be differentiated from conformational changes associated with the loss of active site phosphate.

At a global level, the structure of *B. cereus* PPM in the $P2_12_12_1$ space group (Figure 1) appears to be similar to the structure determined in the previously reported $P2_1$ space group. Superposition of the individual domains of PPM determined from the protein crystallized in the $P2_12_12_1$ space group with the structures of the equivalent domains determined from the previously published $P2_1$ space group (PDB entry 3M8W[6]) resulted in a root-mean-square deviation (rmsd) for C_α atoms of the core domain of 0.5 Å, and an rmsd for C_α atoms of the cap domain of 0.3 Å.

Although the folds of the individual domains of both phosphorylated and unphosphorylated PPM are statistically identical, an interdomain angle change accompanied the loss of active site phosphorylation (Figure 5). The angles of interdomain reorganization in *B. cereus* PPM are restricted to two directions, twist and closure, by the main chain backbone that acts as the hinge (Figure 5A). Comparisons between unphosphorylated PPM and phosphorylated PPM show that the unphosphorylated enzyme is associated with an 18° twist and a 4° closure of the cap domain relative to the core domain (Figure 5B and Video 1 of the Supporting Information). Conversely, a comparison of the phosphorylated structure of *B. cereus* PPM determined in the $P2_12_12_1$ space group to the previously reported phosphorylated PPM in the $P2_1$ space group (PDB entries 3M8W, 3M8Y, 3M8Z, and 3OTY[6]) showed only a 2° twist and a 1° closure of the cap domain relative to the core domain.

In *B. cereus* PPM, the interdomain contacts (Figure 6A) appear to be dictated by three types of molecular interactions: hydrophobic interactions, hydrogen bonding interactions, and metal coordination. The most extensive interaction mediating the interdomain interface is a hydrophobic cluster containing side chains from both the core and cap domains (Figure 6B and Table 3). These hydrophobic interactions are not significantly altered upon domain rotation. Hydrogen bonding interactions further contribute to the interdomain orientation. Here, a difference is observed with a change in domain angle. Two interdomain hydrogen bonding interactions are observed in phosphorylated PPM, while four interdomain hydrogen bonding interactions are observed in the crystal structure of unphosphorylated PPM (Figure 6C,D and Table 3).

Surprisingly, the interdomain contacts through the active site Mn^{2+} also differ between phosphorylated and unphosphory-

dx.doi.org/10.1021/bi201761h | *Biochemistry* 2012, 51, 1964–1975

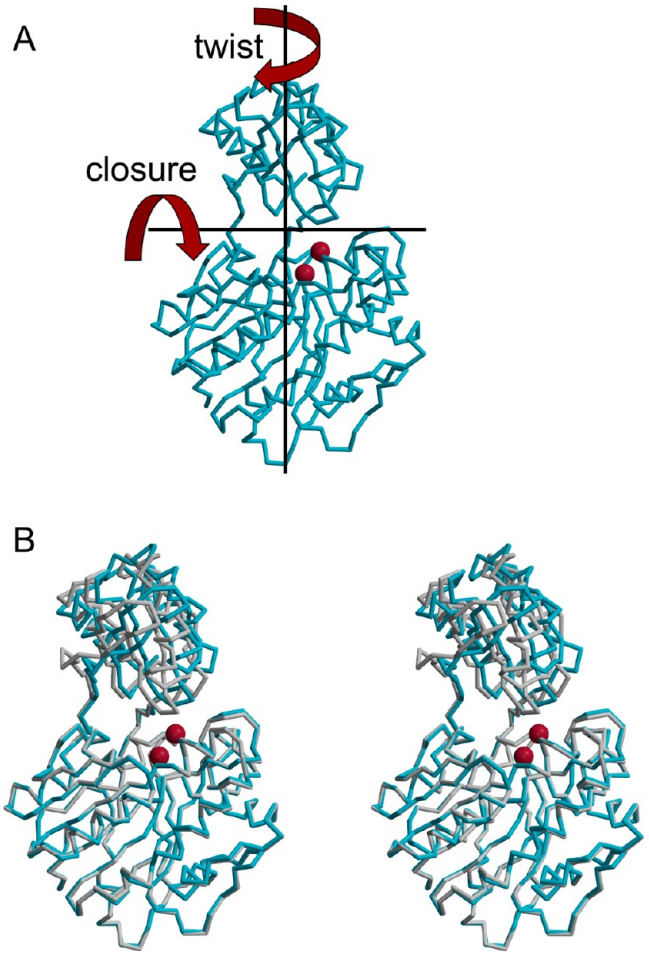

Figure 5. Phosphorylation-dependent interdomain orientation in *B. cereus* PPM. (A) Diagram of the twist and closure axes in relation to the core and cap domains of the structure of PPM. The backbone is represented as a cyan trace, and the Mn^{2+} ions are shown as burgundy spheres. (B) Stereoview of the overlay of the core domains of phosphorylated PPM (cyan) with that of unphosphorylated PPM (gray) demonstrating the relative difference in the orientation of the cap domain in the two states of the enzyme. When the enzymes are divided along the two axes of rotation, 18° of the angle change is around the twist axis while only 4° is around the closure axis.

lated PPM. First, it is noted that comparison between the active site of phosphorylated PPM in the $P2_12_12_1$ space group with that of phosphorylated PPM in the $P2_1$ space group[6] shows no significant differences in metal coordination upon the change in space group (Figure 7A,B). Interestingly, unphosphorylated PPM shows a change in the coordination number and geometry of the Mn-1 ion (Figure 7C). In the phosphorylated enzyme, the O1P atom of p-Thr-85 contributes to the coordination of Mn-1. This ligand is lost in the unphosphorylated enzyme, and a compensatory change in the rotamer of Asp-156 is observed. In the new conformation, the side chain Oδ2 atom remains a ligand to Mn-1, and Oδ1 now forms a hydrogen bonding interaction with Oγ of unphosphorylated Thr-85. This change in side chain conformation converts Mn-1 from a five-coordinate distorted square pyramidal geometry to a four-coordinate distorted tetrahedral geometry. Outside of the change in the rotamer of Asp-156, the active site side chains of unphosphorylated *B. cereus* PPM do not show any significant changes in conformation.

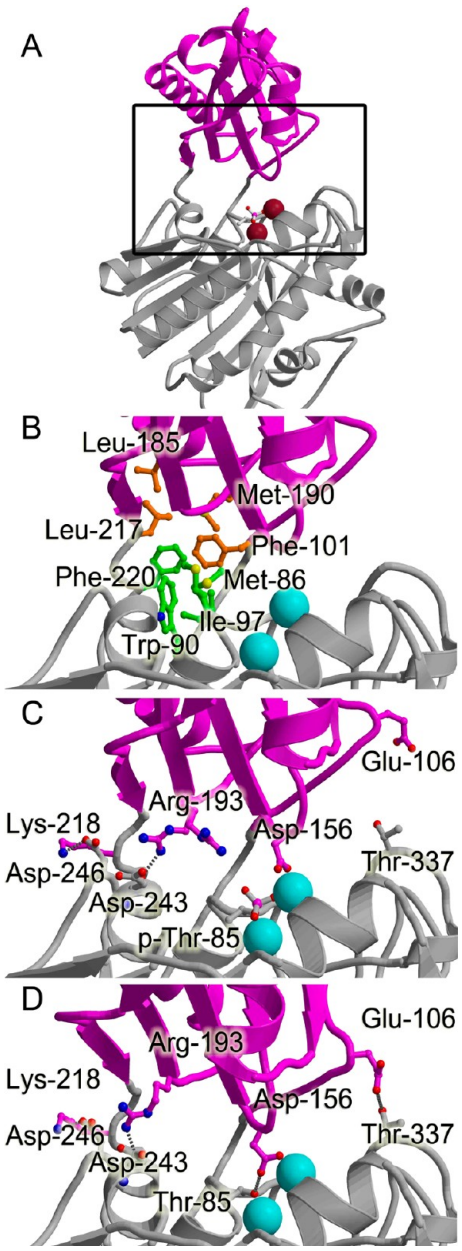

Figure 6. Contacts stabilizing the interdomain orientation in phosphorylated and unphosphorylated *B. cereus* PPM. All panels have the core domain colored gray and the cap domain magenta. (A) Global view of *B. cereus* PPM with Mn^{2+} ions highlighted in cyan and p-Thr-85 depicted as a stick model. The region highlighted in panels B–D is delineated in the box. (B) Highlight of the hydrophobic cluster of residues stabilizing the interdomain contacts. Residues emanating from the core domain are colored green and residues emanating from the cap domain orange. (C) Interdomain hydrogen bonding interactions in phosphorylated *B. cereus* PPM. The structure of PPM determined from the $P2_12_12_1$ crystal form is shown, but the hydrogen bonding interactions are unchanged between the $P2_12_12_1$ crystal form and the $P2_1$ crystal form. (D) Interdomain hydrogen bonding interactions in unphosphorylated *B. cereus* PPM.

Roles for Lys-240 and Asp-156 in Activation. The studies of the PPM^{T85E} and PPM^{T85Q} variants demonstrated that a change in the conformation of Lys-240 influences the affinity for the activator glucose 1,6-bisphosphate (Figures 3 and 4) and suggest a role for this side chain in the activation process. The role of the Asp-156 side chain in activation and

dx.doi.org/10.1021/bi201761h | *Biochemistry* 2012, 51, 1964–1975

Table 3. Interdomain Interactions in Phosphorylated and Unphosphorylated *B. cereus* PPM

phosphorylated			unphosphorylated		
core domain	cap domain	distance (Å)	core domain	cap domain	distance (Å)
		Hydrophobic Cluster[a]			
Met-86	Phe-101		Met-86	Phe-101	
Trp-90	Leu-185		Trp-90	Leu-185	
Ile-97	Met-190		Ile-97	Met-190	
Leu-217			Leu-217		
Phe-220			Phe-220		
		Hydrogen Bonding Interactions[b]			
Asp-243 O	Arg-193 Nη1	2.6	Asp-243 O	Arg-193 Nη2	2.9
Asp-246 Oδ1	Lys-218 Nζ	2.9	Asp-246 Oδ1	Lys-218 Nζ	2.9
			Thr-337 Oγ1	Glu-106 Oδ2	2.9
			Thr-85 Oγ1	Asp-156 Oδ1	2.4
		Interdomain Metal Ligation			
Mn-1	Asp-156 Oδ2	2.1[c]	Mn-1	Asp-156 Oδ2	2.1[c]

[a]Residues in the hydrophobic cluster are listed in numerical order, and the listing of the residues on the same line does not imply specific interactions between the side chains. The indicated side chains form a compact cluster with contributions from all residues. [b]Hydrogen bonding interactions were identified and measured using O.[22] [c]The distance is consistent with metal ligation.

catalysis is less immediately clear. The new orientation of the Asp-156 side chain in the unphosphorylated enzyme partially restricts access to Mn-1 in the active site (compare the location of the Asp-156 side chain in Figure 7C to the location of the phosphate in Figure 7B) but also forms a tight hydrogen bonding interaction with Oγ of Thr-85, which is expected to enhance the nucleophilicity of Oγ and modify its orientation with respect to the glucose 1,6-bisphosphate phosphate donor. This leads to two opposing hypotheses. Asp-156 could be a key residue for enzyme activation by favoring nucleophilic displacement of the glucose 1,6-bisphosphate donor and thereby boosting the steady state phosphorylation of Thr-85. Conversely, by sterically restricting access to Mn-1, Asp-156 could be acting to self-inhibit the enzyme and prevent off-pathway phosphatase activity.

To test these hypotheses, we created the PPM^{D156A} and PPM^{K240A} variants, with the former possibly influencing activation by influencing chemical reactivity and the latter possibly influencing activation by reducing the affinity of PPM for the small molecule activator glucose 1,6-bisphosphate (Figures 3 and 4). Both variants were expressed to levels similar to that of the wild-type enzyme and were folded properly, as assessed by comparing the size exclusion chromatography profiles of the wild-type enzyme, PPM^{K240A}, and PPM^{D156A} (data not shown). None of the variant enzymes exhibited detectable phosphopentomutase activity under the conditions tested (data not shown). We used Western analysis to assess the ability of these variants to be phosphorylated. Excitingly, the PPM^{D156A} variant displays a dramatically reduced level of phosphorylation of the active site Thr-85, while both the wild-type enzyme and the PPM^{K240A} variant can be phosphorylated by the small molecule activator glucose 1,6-bisphosphate (Figure 8). This suggests that the hydrogen bonding interaction between Asp-156 and Thr-85 in the unphosphorylated enzyme is important for activation by glucose 1,6-bisphosphate, and that the influence of the Lys-240 side chain is less important in the activation process. Interestingly, the PPM^{K240A} variant appears to be phosphorylated more readily than the wild-type enzyme. The fact that the PPM^{K240A} variant retains the ability to be robustly phosphorylated (Figure 8) yet lacks catalytic activity suggests that this side chain plays an additional mechanistic role in the catalytic cycle that is presently being investigated.

We next tested whether the Asp-156 side chain influenced the reaction outcome (Figure 2) by restricting access to Mn-1 when PPM is unphosphorylated (Figure 7C). If this were true, removal of this restriction could be sufficient to convert PPM to a phosphatase. Accordingly, we assessed the rate of phosphate hydrolysis of ribose 5-phosphate and glucose 1,6-bisphosphate by both wild-type PPM and PPM^{D156A}. We did not detect an increase in phosphatase activity in the PPM^{D156A} variant as compared to the wild-type enzyme (data not shown). The fact that the PPM^{D156A} variant did not acquire phosphatase activity suggests that the Asp-156 side chain is unlikely to sterically prevent phosphatase activity in unactivated PPM. Instead, additional differences between PPM and alkaline phosphatase likely tune these related enzymes to perform their respective reactions.

DISCUSSION

Mechanisms of Activation of *B. cereus* PPM. In general, enzymes classified within a superfamily have similar structures and catalytic mechanisms. For example, in the catalytic cycle of the cofactor-independent phosphoglycerate mutase, which belongs to the alkaline phosphatase family, it has been concluded that the enzyme follows the same catalytic cycle as alkaline phosphatase (Figure 2B) despite having an overall reaction more similar to that of PPM. The reaction cycle of cofactor-independent phosphoglycerate mutase results in the transfer of a phosphoryl group from one position on the substrate molecule to a second position in the same molecule[31] via an intermediate with the enzyme transiently phosphorylated and the substrate transiently unphosphorylated. In this case, the incoming substrate, rather than a water molecule, acts as the phosphoryl acceptor[32] (Figure 2B, steps 5 and 6). This defines cofactor-independent phosphoglycerate mutase as an intramolecular mutase.

Because sequence and structural analyses place PPM within the alkaline phosphatase superfamily, one of the most intriguing surprises was the observation of a mechanistic deviation between PPM and other biochemically characterized members of the alkaline phosphatase family, including other characterized mutases within the alkaline phosphatase family. Alkaline

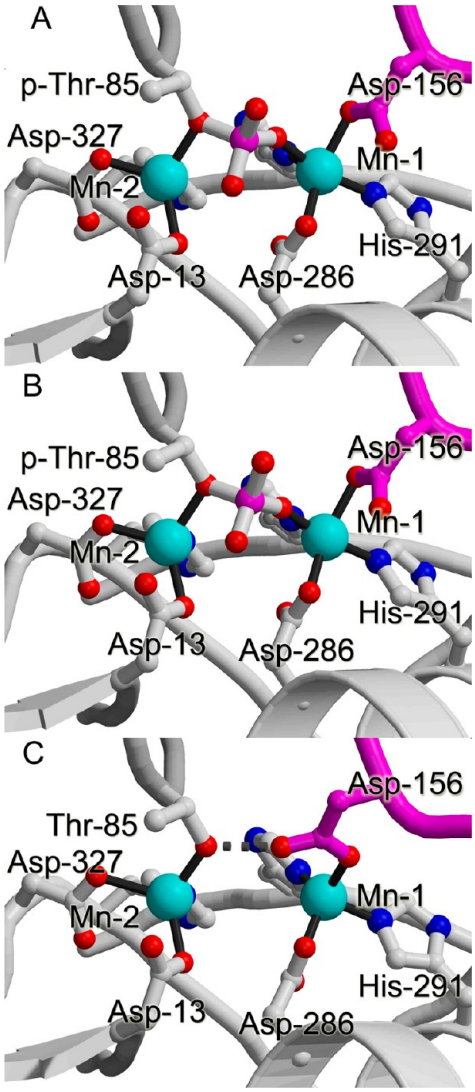

Figure 7. Active site of phosphorylated and unphosphorylated PPM. The active site of PPM is colored with both backbone and carbons emanating from the core domain (gray) and with backbone and carbons emanating from the cap domain (magenta). Mn^{2+} ions are shown as cyan spheres. Metal ligation (<2.2 Å) is shown as solid black lines, and hydrogen bonds are shown as dashed gray lines. The side chain of Asp-286, a metal ligand to Mn-2, has been omitted from all figure panels for the sake of clarity. (A) Active site of phosphorylated *B. cereus* PPM in the $P2_1$ crystal form.[6] (B) Active site of phosphorylated *B. cereus* PPM in the $P2_12_12_1$ crystal form. (C) Active site of unphosphorylated *B. cereus* PPM in the $P2_12_12_1$ crystal form. Note the movement of the Asp-156 ligand and the newly formed hydrogen bonding interaction with Thr-85.

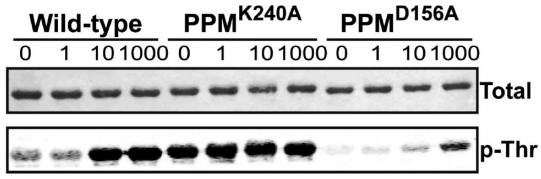

Figure 8. Western analysis of phosphothreonine levels of wild-type and variant *B. cereus* PPM after incubation with glucose 1,6-bisphosphate. The top panel (labeled Total) shows the Ponceau S-stained nitrocellulose membrane, which confirms equal protein loading between lanes. The bottom panel (labeled p-Thr) shows the Odyssey image of the same nitrocellulose membrane following incubation with a phosphothreonine-specific primary antibody and an AlexaFluor680-labeled secondary antibody. The concentration of glucose 1,6-bisphosphate (in micromolar) and enzyme identity are indicated above the lanes.

phosphatase is catalytically active when the active site nucleophile is unphosphorylated, and the reaction proceeds through a transiently phosphorylated catalytic intermediate (Figure 2B). Conversely, PPM is catalytically active when the active site nucleophile is phosphorylated, and the reaction proceeds through a transiently unphosphorylated intermediate[6] (Figure 2A), making it an intermolecular mutase. *B. cereus* PPM is the only characterized member of the alkaline phosphatase family for which this difference in the catalytic cycle has been demonstrated. To diverge from the alkaline phosphatase catalytic cycle, one requirement is that PPM must have a mechanism for the phosphorylation of the active site nucleophile. These studies investigate that mechanism.

The active site ligands to the dimetallo center are absolutely conserved between PPM and alkaline phosphatase with the exception of Asp-156, which is unique to PPM.[6] Because no previously characterized member of the alkaline phosphatase superfamily has a side chain equivalent to Asp-156 ligating the metallo center, the presence of this additional ligand is unexpected. In our previous studies, we identified that binding of the substrate, ribose 5-phosphate (PDB entry 3M8Z[6]), resulted in the side chain of Asp-156 adopting an alternative conformation where its carboxylate was 4.5 Å from Mn-1, which is too far for it to act as a ligand. This strongly suggests that the predominant role of Asp-156 is not in metal binding. The structure of unphosphorylated PPM revealed that the side chain of Asp-156 forms a tight hydrogen bonding interaction with Oγ of the unphosphorylated active site nucleophile, Thr-85 (Figure 7C). This is predicted to both enhance the reactivity of Oγ of Thr-85, which is more sterically hindered than its serine congener in the alkaline phosphatases, and aid in positioning this residue for the catalytic requirement of an in-line attack of glucose 1,6-bisphosphate, which would allow it to become phosphorylated more readily. Indeed, mutation of Asp-156 dramatically reduces the level of enzyme activation by glucose 1,6-bisphosphate (Figure 8). It therefore seems possible that the crystal structure of the unphosphorylated enzyme reflects the conformation of the enzyme after protein synthesis and prior to the first activation.

The poising of Asp-156 in an orientation that activates Thr-85 is associated with a large interdomain rotation. Hints at a possible mechanism for stabilizing the interdomain angle change come from careful examination of the phosphorylated and unphosphorylated PPM structures, which have been determined at resolutions sufficient to model alternate side chain conformations confidently. Importantly, Met-86, Asp-156, and Arg-193, all residues that mediate the interdomain contacts, have been observed in alternate conformations in crystal structures presented here (Figure 6) and previously.[6] A combination of the changes in the conformation of these side chains and the rotation of the domains results in the unphosphorylated form of *B. cereus* PPM containing an increased number of interdomain hydrogen bonds compared to the number in the phosphorylated enzyme (Figure 6B,C and Table 3).

Interestingly, the structure of the PPM^{T85Q} variant did not show a similar change in interdomain angle but instead only

dx.doi.org/10.1021/bi201761h | *Biochemistry* 2012, 51, 1964–1975

showed a change in the conformation of the Lys-240 side chain (Figure 3). There are multiple possibilities for why this could be so. First, the glutamine chain may sterically prevent the interdomain rotation as these are each similar in size to p-Thr. In addition, the structure of the PPM^{T85Q} variant was determined in a crystal form that constrained the orientation of the domains with respect to each other. By comparison, the structure of the fully unphosphorylated enzyme was determined from a crystal form in which packing did not constrain the interdomain orientation. It is therefore possible that the PPM^{T85Q} variant could be in conformational equilibrium in solution, with some enzymes having the domain orientation observed in the crystal structure reported here and some having rotated domains, but that the crystallization conditions selected for those members of the population with their domains similar to those of the activated enzyme.

Perhaps the most interesting possibility for a mechanism favoring Thr-85 phosphorylation incorporates both structural observations. During one type of unproductive turnover in PPM, a bisphosphorylated product could diffuse from the active site and leave unphosphorylated enzyme (Figure 2A; diffusion would occur between steps 3 and 5). A fast conformational change in the Lys-240 side chain is associated with a modest increase in the affinity for the activator glucose 1,6-bisphosphate (Figures 3 and 4) and could increase the likelihood that the PPM could be rephosphorylated quickly. In the absence of activator, the enzyme could then undergo a larger, slower conformational change that more substantially increases the likelihood of rephosphorylation upon the next encounter with glucose 1,6-bisphosphate. Combined, these two mechanisms for improving activation of PPM enhance the affinity for the small molecule activator and increase the reactivity of the Thr-85 nucleophile. Whether these are the only factors that favor an increased level of Thr-85 phosphorylation is presently unknown.

Possible Additional Roles for Interdomain Angle Changes. Enzymes with a global architecture similar to that of PPM, with an active site at an interdomain interface, commonly have angle changes between the domains that can be important for function. Interdomain closure is frequently proposed to accompany catalysis (see, for example, refs 33−38). For example, β-phosphoglucomutase is a member of the haloacid dehalogenase superfamily with mechanistic similarities to PPM despite a lack of sequence identity. In β-phosphoglucomutase, comparison of crystal structures determined in the presence[39] or absence[40] of a transition state analogue altered the orientation of domains relative to each other. The interdomain angle change of unphosphorylated *B. cereus* PPM is predominantly a twist of the cap domain. However, both the $P2_12_12_1$ crystal form presented here and molecules of the previously reported $P2_1$ crystal form have small angle changes (<2°) along the axis of closure. This direction of angle change hints at the possibility that interdomain closure could accompany catalysis, which is the subject of ongoing study.

■ ASSOCIATED CONTENT

Supporting Information

One figure and one video. This material is available free of charge via the Internet at http://pubs.acs.org.

Accession Codes

The atomic coordinates and structure factors for all structures have been deposited in the Protein Data Bank as entries 3TWZ, 3TX0, 3UN2, 3UN3, 3UN5, 3UNY, and 3UO0.

■ AUTHOR INFORMATION

Corresponding Author

*Fax: (615) 343-6532. Phone: (615) 322-7817. E-mail: tina.iverson@vanderbilt.edu.

Present Address

‖Monsanto Co., Chesterfield, MO 63017.

Funding

This work was supported by National Institutes of Health (NIH) Grants GM077189 (B.O.B.), AI079558 (T.M.I.), and GM077189 (T.M.I.), pilot project funds from the Vanderbilt Institute of Chemical Biology (B.O.B.), and NIH Training Grants T32 NS07491 (T.D.P.), T32 GM008320 (T.D.P.), T32 GM065086 (W.R.B.), and T90 DA022873 (D.P.N.).

Notes

The authors declare no competing financial interest.

■ ACKNOWLEDGMENTS

Use of the LS-CAT beamlines at the Advanced Photon Source was supported by the U.S. Department of Energy, Office of Science, Office of Basic Energy Sciences, under Contract DE-AC02-06CH11357. Portions of this research were conducted at the Stanford Synchrotron Radiation Lightsource (SSRL), a national user facility operated by Stanford University on behalf of the U.S. Department of Energy, Office of Basic Energy Sciences. The SSRL Structural Molecular Biology Program is supported by the Department of Energy, Office of Biological and Environmental Research, and by the National Institutes of Health, National Center for Research Resources, Biomedical Technology Program, and the National Institute of General Medical Sciences. A portion of this work used facilities that were supported by the Vanderbilt Core Grant in Vision Research (P30EY008126). We thank Brian Wadzinski for use of facilities and reagents, Kathryn McCulloch and Tarjani Thaker for critical reading, and Kathryn McCulloch, Allyson McLeod, and Rey Gomez for experimental assistance.

■ REFERENCES

(1) Tozzi, M. G., Camici, M., Mascia, L., Sgarrella, F., and Ipata, P. L. (2006) Pentose phosphates in nucleoside interconversion and catabolism. *FEBS Lett. 273*, 1089−1101.

(2) Hammer-Jespersen, K., and Munch-Petersen, A. (1970) Phosphodeoxyribomutase from *Escherichia coli*: Purification and some properties. *Eur. J. Biochem. 17*, 397−407.

(3) Kammen, H. O., and Koo, R. (1969) Phosphopentomutaes. I. Identification of two activities in rabbit tissues. *J. Biol. Chem. 244*, 4888−4893.

(4) Galperin, M. Y., Bairoch, A., and Koonin, E. V. (1998) A superfamily of metalloenzymes unifies phosphopentomutase and cofactor-independent phosphoglycerate mutase with alkaline phosphatases and sulfatases. *Protein Sci. 7*, 1829−1835.

(5) Maliekal, P., Sokolova, T., Vertommen, D., Veiga-Da-Cunha, M., and Van Schaftingen, E. (2007) Molecular identification of mammalian phosphopentomutase and glucose-1,6-bisphosphate synthase, two members of the α-D-phosphohexomutase family. *J. Biol. Chem. 282*, 31844−31851.

(6) Panosian, T. D., Nannemann, D. P., Watkins, G. R., Phelan, V. V., McDonald, W. H., Wadzinski, B. E., Bachmann, B. O., and Iverson, T. M. (2011) *Bacillus cereus* phosphopentomutase is an alkaline

phosphatase family member that exhibits an altered entry point into the catalytic cycle. *J. Biol. Chem. 286*, 8043−8054.
(7) Ghosh, S. S., Bock, S. C., Rokita, S. E., and Kaiser, E. T. (1986) Modification of the active site of alkaline phosphatase by site-directed mutagenesis. *Science 231*, 145−148.
(8) Plocke, D. J., Levinthal, C., and Valee, B. L. (1962) Alkaline phosphatase of *Escherichia coli*: Zinc metalloenzyme. *Biochemistry 1*, 373−378.
(9) Kim, E. E., and Wyckoff, H. W. (1991) Reaction mechanism of alkaline phosphatase based on crystal structures: Two-metal ion catalysis. *J. Mol. Biol. 218*, 449−464.
(10) Coleman, J. E. (1992) Structure and mechanism of alkaline-phosphatase. *Annu. Rev. Biophys. Biomol. Struct. 21*, 441−483.
(11) Panosian, T. D., Nannemann, D. P., Bachmann, B. O., and Iverson, T. M. (2010) Crystallization and preliminary X-ray analysis of a phosphopentomutase from *Bacillus cereus*. *Acta Crystallogr. F66*, 811−814.
(12) Otwinowski, Z., and Minor, W. (1997) Processing of X-ray diffraction data collected in oscillation mode. *Methods Enzymol. 276*, 307−326.
(13) Collaborative Computational Project Number 4 (1994) The CCP4 Suite: Programs for protein crystallography. *Acta Crystallogr. D50*, 760−763.
(14) Brunger, A. T. (2007) Version 1.2 of the Crystallography and NMR system. *Nat. Protoc. 2*, 2728−2733.
(15) McCoy, A. J., Grosse-Kunstleve, R. W., Adams, P. D., Winn, M. D., Storoni, L. C., and Read, R. J. (2007) Phaser crystallographic software. *J. Appl. Crystallogr. 40*, 658−674.
(16) Emsley, P., and Cowtan, K. (2004) Coot: Model-building tools for molecular graphics. *Acta Crystallogr. D60*, 2126−2132.
(17) Murshudov, G. N., Vagin, A. A., and Dodson, E. J. (1997) Refinement of macromolecular structures by the maximum-likelihood method. *Acta Crystallogr. D53*, 240−255.
(18) Vagin, A. A., Steiner, R. A., Lebedev, A. A., Potterton, L., McNicholas, S., Long, F., and Murshudov, G. N. (2004) REFMAC5 dictionary: Organization of prior chemical knowledge and guidelines for its use. *Acta Crystallogr. D60*, 2184−2195.
(19) Winn, M. D., Isupov, M. N., and Murshudov, G. N. (2001) Use of TLS parameters to model anisotropic displacements in macromolecular refinement. *Acta Crystallogr. D57*, 122−133.
(20) Painter, J., and Merritt, E. A. (2006) TLSMD web server for the generation of multi-group TLS models. *J. Appl. Crystallogr. 39*, 109−111.
(21) Hayward, S., and Berendsen, H. J. C. (1998) Systematic analysis of domain motions in proteins from conformational change: New results on citrate synthase and T4 lysozyme. *Proteins 30*, 144−154.
(22) Jones, T. A., Zou, J. Y., Cowan, S. W., and Kjeldgaard, M. (1991) Improved methods for building protein models in electron density maps and the location of errors in these models. *Acta Crystallogr. A47*, 110−119.
(23) Kraulis, P. J. (1991) MOLSCRIPT: A program to produce both detailed and schematic plots of protein structures. *J. Appl. Crystallogr. 24*, 946−950.
(24) Esnouf, R. M. (1999) Further additions to MolScript version 1.4, including reading and contouring of electron-density maps. *Acta Crystallogr. D55*, 938−940.
(25) Merritt, E. A., and Bacon, D. J. (1997) Raster3D photorealistic molecular graphics. *Methods Enzymol. 277*, 505−524.
(26) Delano, W. L. (2002) *The PyMOL Molecular Graphics System*, DeLano Scientific, Palo Alto, CA.
(27) Ball, E. G. (1939) Xanthine oxidase: Purification and properties. *J. Biol. Chem. 128*, 51−67.
(28) Nannemann, D. P., Kaufmann, K. W., Meiler, J., and Bachmann, B. O. (2010) Design and Directed Evolution of a Dideoxy Purine Nucleoside Phosphorylase. *Protein Eng., Des. Sel. 23*, 607−616.
(29) de Groot, H., and Noll, T. (1985) Enzymatic determination of inorganic phosphates, organic-phosphates and phosphate-liberating enzymes by use of nucleoside phosphorylase xanthine-oxidase (dehydrogenase)-coupled reactions. *Biochem. J. 230*, 255−260.
(30) Scism, R. A., Stec, D. F., and Bachmann, B. O. (2007) Synthesis of nucleotide analogues by a promiscuous phosphoribosyltransferase. *Org. Lett. 9*, 4179−4182.
(31) Gatehouse, J. A., and Knowles, J. R. (1977) Phosphoglycerate mutase from wheat-germ: Studies with isotopically labelled 3-phospho-D-glycerates showing that the catalyzed reaction is intramolecular. *Biochemistry 16*, 3045−3050.
(32) Galperin, M. Y., and Jedrzejas, M. J. (2001) Conserved core structure and active site residues in alkaline phosphatase superfamily enzymes. *Proteins 45*, 318−324.
(33) Tomasiak, T. M., Maklashina, E., Cecchini, G., and Iverson, T. M. (2008) A threonine on the active site loop controls transition state formation in *Escherichia coli* respiratory complex II. *J. Biol. Chem. 283*, 15460−15468.
(34) Chuang, G. Y., Mehra-Chaudhary, R., Ngan, C. H., Zerbe, B. S., Kozakov, D., Vajda, S., and Beamer, L. J. (2010) Domain motion and interdomain hot spots in a multidomain enzyme. *Protein Sci. 19*, 1662−1672.
(35) Shan, L., Mathews, I. I., and Khosla, C. (2005) Structural and mechanistic analysis of two prolyl endopeptidases: Role of interdomain dynamics in catalysis and specificity. *Proc. Natl. Acad. Sci. U.S.A. 102*, 3599−3604.
(36) Barycki, J. J., O'Brien, L. K., Strauss, A. W., and Banaszak, L. J. (2000) Sequestration of the active site by interdomain shifting. Crystallographic and spectroscopic evidence for distinct conformations of L-3-hydroxyacyl-CoA dehydrogenase. *J. Biol. Chem. 275*, 27186−27196.
(37) Longenecker, K. L., Stamper, G. F., Hajduk, P. J., Fry, E. H., Jakob, C. G., Harlan, J. E., Edalji, R., Bartley, D. M., Walter, K. A., Solomon, L. R., Holzman, T. F., Gu, Y. G., Lerner, C. G., Beutel, B. A., and Stoll, V. S. (2005) Structure of MurF from *Streptococcus pneumoniae* co-crystallized with a small molecule inhibitor exhibits interdomain closure. *Protein Sci. 14*, 3039−3047.
(38) Hayward, S. (2004) Identification of specific interactions that drive ligand-induced closure in five enzymes with classic domain movements. *J. Mol. Biol. 339*, 1001−1021.
(39) Lahiri, S. D., Zhang, G. F., Dunaway-Mariano, D., and Allen, K. N. (2003) The pentacovalent phosphorus intermediate of a phosphoryl transfer reaction. *Science 299*, 2067−2071.
(40) Zhang, G. F., Dai, J., Wang, L. B., Dunaway-Mariano, D., Tremblay, L. W., and Allen, K. N. (2005) Catalytic cycling in β-phosphoglucomutase: A kinetic and structural analysis. *Biochemistry 44*, 9404−9416.